Low Frequency Mobile Communications in Underwater Networks

Abdel-Mehsen Ahmad[1], Michel Barbeau[2][0000−0003−3531−4926], Joaquin Garcia-Alfaro[3][0000−0002−7453−4393], Jamil Kassem[1], Evangelos Kranakis[2][0000−0002−8959−4428], and Steven Porretta[2]

[1] School of Engineering, Lebanese International University, Bekaa, Lebanon.
[2] School of Computer Science, Carleton University, Ottawa, ON, Canada, K1S 5B6.
[3] Telecom SudParis, CNRS Samovar, UMR 5157, Evry, France.

Abstract. We present a receiver for low frequency underwater acoustic communications addressing the Doppler shift that occurs during the transmission of frames at a very low data rate. The receiver handles constant or variable (linearly and nonlinearly) Doppler shift patterns. The waveform supported by the receiver is adapted to difficult underwater channel conditions, such as the ones present in long range under-ice Arctic communications. The bandwidth is extremely narrow (less than six Hz). Redundancy is very high (300%). Our main contributions are in an aspect of the receiver that handles arbitrary types of Doppler shifts. We use the idea of signal tracking function. It follows the progression of a carrier during the reception of a frame. Evaluation results are reported using our GNU Radio implementation.

1 Introduction

Underwater data communications and networking have applications in monitoring and surveillance of coastal waters [1], submarine activity sensors [2], autonomous undersea vehicles [3] and submerged airplane locator beacons [4]. We focus on low frequency mobile communications [5,6], i.e., in the range 0.3 to 3 kHz. Relative to higher frequencies, Stojanovic stressed that attenuation is lower [7]. Hence, there is potential for long distance contacts [8]. However, because of the narrow half-power bandwidth of low frequency and long distance operation, only extremely low data rates are possible. Furthermore, the relative mobility of a transmitter and a receiver affects the acoustic waves used for underwater communications. This is the Doppler effect. Contrasted with classical electromagnetic communications, it has a significant impact.

In this paper, we consider the Doppler shift that occurs during the reception of low-data rate frames in low frequency and long distance acoustic underwater communications. There are three cases: constant, linearly variable and nonlinearly variable Doppler shift. In background research [9,10], we concluded that in the case of transmitter-receiver collateral motions, in the zero to eight knot range, we have constant relative velocity and constant Doppler shift within zero to eight Hz. For transverse motions, the Doppler effect is nonlinearly variable in

time. For a transmitter carried by a meandering current and a vertically oscillating receiver, the Doppler effect is nonlinearly variable in time, up to 35 Hz. Regarding a transmitter in a diagonal oscillation, the Doppler shift is nonlinearly variable in time (up to 15 Hz), decreasing with elevation. Finally, when multiple receivers are in motion, they observe different shifts.

We propose a receiver that handles constant, linearly variable or nonlinearly variable Doppler shifts. The type of signal and data encoding produced by the protocol supported by the receiver are suitable for harsh conditions (e.g., long range and long distance Arctic communications). The bandwidth is extremely narrow. The signal occupies less than six Hz. Forward Error Correction (FEC) with 300% redundancy and probabilistic decoding are used. Our main contribution is in the receiver design. Decoding is done in three steps: energy search, synchronization and demodulation. The demodulator generates soft symbols. Each bit a superposition of zero or one, with a certain probability for each value. Considering the most probable values first, the decoder tries to obtain a valid frame (which passes error correction). If it does not work, other possibilities are tried. The number of attempts is controlled (by a parameter). This type of decoding was invented by Fano [11]. Classical decoding uses Viterbi, much faster and less complex, but it cannot tolerate high error rates as Fano. In the case of underwater communications, Fano is suitable because the data rates are very low. The computer is very fast relative to the channel speed and can spend a lot of time decoding and searching for signals. To handle arbitrary forms of Doppler shift, we introduce the concept of signal tracking function that models the evolution of a carrier during the reception of a frame.

Section 2 covers the channel model. A trajectory model that yields nonlinearly changing Doppler shift patterns is presented in Section 3. The detailed receiver design is discussed in Section 4. We elaborate our evaluation approach and review simulation results in Section 5. We conclude with Section 6.

2 Channel Model

This paper builds upon a Doppler shift analysis [9,10] and a protocol design for communications with slow-rate data frames carried by low frequency underwater acoustic signals [12]. The protocol already handles constant or linearly variable Doppler shifts. It does not handle nonlinearly variable Doppler shift. The goal of the work presented in this paper is to extend the protocol in [12] to handle nonlinearly variable Doppler shifts.

Let $v(t)$ be the relative speed (m/s) between a transmitter and a receiver at time t. Let c be the signal propagation speed (m/s). At nominal frequency f_0 Hz, the Doppler effect causes a frequency shift defined is

$$f_\Delta(t) = f_0 \frac{v(t)}{c} \text{ Hz.} \tag{1}$$

Let $x(t)$, $y(t)$ and $w(t)$ denote the transmitted baseband signal, received signal, and additive white Gaussian noise. As a function of time, the level of the received

signal is $y(t) = \alpha e^{-\sqrt{-1}\theta(t)} x(t) + w(t)$. Attenuation is represented by factor α. Doppler shift is modelled in the phase term $\theta(t) = 2\pi \left[f_0 + f_\Delta(t)\right] t$ rad. Constant Doppler shift means that the function f_Δ is constant during reception of a frame. The transmitter-receiver relative speed ($v(t)$) is constant, as a function of time. Linearly variable Doppler shift implies that during the reception of a frame the value f_Δ is variable, but can be modelled by a first degree polynomial. For the nonlinear case, f_Δ is an arbitrary function and cannot be modelled by a first degree polynomial.

3 Trajectory Model

We study and model trajectories, of underwater vehicles, producing nonlinearly variable Doppler shifts.

Consider two vehicles R_a, R_b moving along trajectories defined in the Euclidean space[4]

$$t \to \boldsymbol{A}(t) = (A_1(t), A_2(t), A_3(t)) \text{ and } t \to \boldsymbol{B}(t) = (B_1(t), B_2(t), B_3(t)) \qquad (2)$$

such that at time t they occupy positions $\boldsymbol{A}(t), \boldsymbol{B}(t)$ while moving with constant speeds v_a, v_b, respectively (see Figure 1). Each trajectory is a smooth, rectifiable,

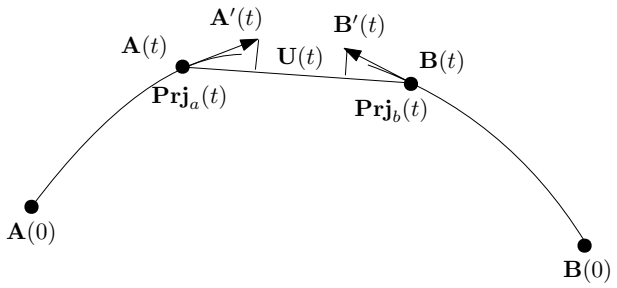

Fig. 1. Movement of the vehicles along their corresponding smooth, rectilinear trajectories $t \to \boldsymbol{A}(t)$ and $t \to \boldsymbol{B}(t)$.

and non-crossing curve. Since the two vehicles move with constant speeds, by time t they must have covered a trajectory of length $v_a t, v_b t$, respectively, and therefore the following two equations are valid

$$v_a t = \int_0^t \|\boldsymbol{A'}(s)\| ds \text{ and } v_b t = \int_0^t \|\boldsymbol{B'}(s)\| ds, \qquad (3)$$

[4] An analogous formulation using two instead of three cartesian coordinates is possible in the Euclidean plane.

where $\boldsymbol{A'}(s), \boldsymbol{B'}(s)$ denote the derivatives of $\boldsymbol{A}(s), \boldsymbol{B}(s)$, with respect to the variable s, and $\|\boldsymbol{A'}(t)\|, \|\boldsymbol{B'}(t)\|$ is the norm of these vectors in Euclidean space. From the fundamental theorem of calculus and Equation (3), it follows that $v_a = \|\boldsymbol{A'}(t)\|$ and $v_b = \|\boldsymbol{B'}(t)\|$, for all $t \geq 0$.

We project $\boldsymbol{A'}(t)$ and $\boldsymbol{B'}(t)$ onto the vector $\boldsymbol{U}(t) = \boldsymbol{B}(t) - \boldsymbol{A}(t)$ as depicted in Figure 1, thus forming the corresponding projection vectors $\boldsymbol{Prj}_a(t)$ and $\boldsymbol{Prj}_b(t)$. They yield the following formula for the projection vector $\boldsymbol{Prj}_a(t)$ of $\boldsymbol{A'}(t)$ on the vector $\boldsymbol{U}(t)$,

$$\boldsymbol{Prj}_a(t) = \|\boldsymbol{A'}(t)\| \cdot \frac{< \boldsymbol{A'}(t), \boldsymbol{U}(t) >}{\|\boldsymbol{A'}(t)\| \cdot \|\boldsymbol{U}(t)\|} \cdot \frac{\boldsymbol{U}(t)}{\|\boldsymbol{U}(t)\|} = \frac{< \boldsymbol{A'}(t), \boldsymbol{U}(t) >}{\|\boldsymbol{U}(t)\|} \cdot \frac{\boldsymbol{U}(t)}{\|\boldsymbol{U}(t)\|}$$

where $< \cdot, \cdot >$ denotes the inner product of vectors. They yield a similar formula for the projection vector $\boldsymbol{Prj}_b(t)$ of $\boldsymbol{B'}(t)$ on the vector $\boldsymbol{U}(t)$. Subtracting the projection vectors and using the fact that the inner product is bilinear we see that

$$\boldsymbol{Prj}_a(t) - \boldsymbol{Prj}_b(t) = \frac{< \boldsymbol{A'}(t) - \boldsymbol{B'}(t), \boldsymbol{U}(t) >}{\|\boldsymbol{U}(t)\|} \cdot \frac{\boldsymbol{U}(t)}{\|\boldsymbol{U}(t)\|}. \tag{4}$$

Using Formulas (4) and (1), we derive the Doppler effect resulting from the movement of the two vehicles in Theorem 1.

Theorem 1 (Doppler Effect). *For two vehicles R_a, R_b moving in Euclidean space with constant speeds v_a, v_b on their respective smooth, rectifiable trajectories $t \to \boldsymbol{A}(t)$ and $t \to \boldsymbol{B}(t)$ the change in frequency is*

$$\Delta f(t) = -\text{sign}\left(\|\boldsymbol{U}(t)\|'\right) \cdot \frac{| < \boldsymbol{A'}(t) - \boldsymbol{B'}(t), \boldsymbol{U}(t) > |}{\|\boldsymbol{U}(t)\|} \cdot \frac{f_0}{c} \tag{5}$$

where $|\cdot|$ denotes the absolute value, and f_0 is the transmission frequency and c is the sound speed.

Note that the quantity $-\text{sign}\left(\|\boldsymbol{U}(t)\|'\right)$ is positive when the projection vectors $\boldsymbol{Prj}_a(t), \boldsymbol{Prj}_b(t)$ are pointing towards each other and negative when they are in opposite directions.

We treat now the special case of straight line trajectories. First, we show how to convert the Cartesian representation to the Parametric one. Next, we show how to calculate the Doppler effect from the Parametric representation of straight lines. For simplicity of notation, we give the formulas for the Euclidean plane but similar formulas to Euclidean space.

If the straight lines traversed by the vehicles R_a and R_b are given in standard Cartesian form $y = m_a x + c_a$ and $y = m_b x + c_b$, where m_a, m_b are the slopes of the lines and c_a, c_b are constants, then we can convert them to the parametric form. Let the respective initial positions of the vehicles be $\bar{\boldsymbol{a}} = (\bar{a}_1, \bar{a}_2)$ and $\bar{\boldsymbol{b}} = (\bar{b}_1, \bar{b}_2)$. From the equations of the two lines we see that

$$\bar{a}_2 = m_a \bar{a_1} + c_a \text{ and } \bar{b}_2 = m_b \bar{b_1} + c_b. \tag{6}$$

Let $\boldsymbol{A}(t), \boldsymbol{B}(t)$ be the positions of the vehicles at time t on their respective line trajectories. Further, let $x_a(t), y_a(t)$ and $x_b(t), y_b(t)$ be the horizontal and vertical offsets from their starting positions positions at time t. Observe that since the vehicles are moving with constant speeds their positions satisfy

$$\boldsymbol{A}(t) = (\bar{a}_1 + x_a(t), \bar{a}_2 + y_a(t)) \text{ and } \boldsymbol{B}(t) = (\bar{b}_1 + x_b(t), \bar{b}_2 + y_b(t)), \tag{7}$$

where by assumption, $x_a(0) = y_a(0) = x_b(0) = y_b(0) = 0$. Since the vehicles are moving on straight lines, we have by definition that $y_a(t) = m_a x_a(t)$ and $y_b(t) = m_b x_b(t)$; further, since they are moving with constant speeds we conclude that $x_a^2(t) + y_a^2(t) = (v_a t)^2$. Combining these last two equations, we conclude that the corresponding offsets for vehicle R_a are $x_a(t) = v_a t/\sqrt{1+m_a^2}$ and $y_a(t) = m_a v_a t/\sqrt{1+m_a^2}$. Entirely similar formulas are valid for the vehicle R_b. It follows that the positions of the vehicles at time t are given by the formulas:

$$\boldsymbol{A}(t) = \boldsymbol{a}t + \bar{\boldsymbol{a}} \text{ and } \boldsymbol{B}(t) = \boldsymbol{b}t + \bar{\boldsymbol{b}} \tag{8}$$

where

$$\boldsymbol{a} = \left(\frac{v_a}{\sqrt{1+m_a^2}}, \frac{m_a v_a}{\sqrt{1+m_a^2}}\right) \text{ and } \boldsymbol{b} = \left(\frac{v_b}{\sqrt{1+m_b^2}}, \frac{m_b v_b}{\sqrt{1+m_b^2}}\right). \tag{9}$$

Consider two vehicles R_a and R_b moving along trajectories defined by the straight lines $t \to \boldsymbol{A}(t) := \boldsymbol{a}t + \bar{\boldsymbol{a}}$ and $t \to \boldsymbol{B}(t) := \boldsymbol{b}t + \bar{\boldsymbol{b}}$, where $\boldsymbol{a}, \boldsymbol{b}, \bar{\boldsymbol{a}}, \bar{\boldsymbol{b}}$ are constant vectors in the Euclidean plane. Thus, the initial positions of the vehicles are $\boldsymbol{A}(0) = \bar{\boldsymbol{a}}$ and $\boldsymbol{B}(0) = \bar{\boldsymbol{b}}$. Using elementary calculations and the notation established in Section **??**, we can derive the following:

$$\boldsymbol{A'}(t) = \boldsymbol{a}, \boldsymbol{B'}(t) = \boldsymbol{b} \text{ and } \boldsymbol{U}(t) = (\boldsymbol{b}-\boldsymbol{a})t + \bar{\boldsymbol{b}} - \bar{\boldsymbol{a}} \tag{10}$$

$$\|\boldsymbol{U}(t)\| = \sqrt{\sum_{i=1}^{2}((b_i - a_i)t + (\bar{b}_i - \bar{a}_i))^2} \tag{11}$$

$$\|\boldsymbol{U}(t)\|' = \frac{\sum_{i=1}^{2}(b_i - a_i)}{\sqrt{\sum_{i=1}^{2}((b_i - a_i)t + (\bar{b}_i - \bar{a}_i))^2}} \tag{12}$$

Substituting these formulas into Equation (5), we can determine the following formula for the change in frequency $f_\Delta(t)$ as measured by the Doppler effect in Theorem 1. We summarize this in the following:

Corollary 1.

$$f_\Delta(t) = -\text{sign}\left(\sum_{i=1}^{2}(b_i - a_i)\right) \cdot \frac{|<\boldsymbol{a}-\boldsymbol{b}, (\boldsymbol{b}-\boldsymbol{a})t + \bar{\boldsymbol{b}} - \bar{\boldsymbol{a}}>|}{\sqrt{\sum_{i=1}^{2}((b_i - a_i)t + (\bar{b}_i - \bar{a}_i))^2}} \cdot \frac{f_0}{c}, \tag{13}$$

where f_0 is the transmission frequency and c is the sound speed.

4 Receiver Design

Underwater communications use sound waves. Significant communication impairments include attenuation and numerous sources of noise [7]. For long range communications, attenuation is an important issue. It is due to conversion of acoustic energy into heat and geometrical spreading. Its importance grows with distance and frequency. Hence, for long distances, solely the use of low frequencies can be envisioned. Another important fact is the gradient of the attenuation versus frequency. It limits the operating bandwidth. The half-power bandwidth is commonly used to define cutoff frequencies and bandwidths of filters by using frequency response curves, using 3 dB points in the frequency response of a band-pass filter [13]. At low frequency (in the few kilohertz range) attenuation is low relative to higher frequencies (e.g., 20 kilohertz), but the gradient of the attenuation is high. Consequently, the half-power bandwidth is very narrow, i.e., just a few Hz. Solely narrow-band modulation is possible, i.e., a few Hz.

We revisit the receiver design in [12], addressing low frequency underwater acoustic communications. The sender design is exactly as originally defined in [12], which is based on ideas authored by Taylor and Walker [14], Franke and Taylor [15], Karn [16] and Fano [11]. The associated protocol is asynchronous frame-oriented. Each frame comprises 162 channel symbols, which encode 50 information bits. Convolutional FEC is used, with a constraint of 32 and a rate of 1/2 [11]. Convolutional encoding of the information bits yields 162 bits. They are interleaved with 162 synchronization bits s_i ($i = 1, \ldots, 162$). Every data bit is paired with a synchronization bit. Each pair makes a channel symbol. Modulation is four-tone Multiple Frequency-Shift Keying (MFSK) at 1.46 (375/256) baud. The complex modulation envelope frequencies are -2.2, -0.7, 0.7 and 2.2 Hz, corresponding to channel symbols 0, 1, 2 and 3. The transmission time of a frame is 111 seconds.

The new receiver has the capability to search for frames with possibly linearly or nonlinearly drifting carriers. Audio is captured by a hydrophone, digitized, band pass filtered and centred to zero Hz. Digitized audio processing is done according to a sliding window model. Each window represents 120 seconds of channel data. The next window slides in time for nine seconds. Each two-minute interval of channel data is represented as a series of discrete complex samples $x_0, x_1, \ldots, x_{N-1}$. In the sequel, N is set to 45,000 samples. Hence, the sampling rate f_s is $N/120 = 375$ samples per second (sps). Each channel symbol is represented by 256 samples. A frame consists of 256 samples per symbol times 162 channel symbols, i.e., 41,472 samples.

Each window of channel data is searched for the presence of 111-second frames. Windowed Discrete Fourier Transforms (DFTs) are calculated. Each DFT represents a time interval corresponding to the duration of two symbols, i.e., 512 samples. The size ν of each DFT is 512 bins. The DFTs are calculated from the beginning of a two-minute interval, in steps of half symbol (128 samples). The number of DFTs is: $n = \lfloor N/128 \rfloor - 3 = 348$ DFTs. The term "-3" is present because calculations of windowed DFTs stop before the third to last half-sample. At 375 sps and according to Nyquist criterion, the frequency range

of each DFT is lower than 375/2 Hz, i.e., including the negative frequencies within the range ±187 Hz. From frequency-bin-to-frequency-bin, there is an offset Δf of $375/512 = 0.73$ Hz. Let m be equal to $\lfloor 187 \cdot \nu / f_s \rfloor = 255$. Every coefficient of the DFTs is denoted as $X_{i,j}$, with the window index i in the range $0, \ldots, n-1$ and frequency index j in the range $-m+1, \ldots, 0, \ldots, m-1$. Every DFT coefficient is defined as:

$$X_{i,j} = \sum_{t=0}^{\nu-1} x_{128i+t} \cdot w(t) \cdot e^{-\sqrt{-1} \cdot 2\pi j t / \nu} \tag{14}$$

where $w(t) = \sin\left(\frac{\pi}{512} \cdot t\right)$ is the windowing function. Equation (14) represents the relative amplitude and phase of frequency $\frac{j \cdot f_s \text{ sps}}{\nu \text{ samples}}$ Hz. In the frequency domain, every two-minute time interval is represented by the following matrix:

$$X = \begin{bmatrix} X_{0,-m+1} & \ldots & X_{0,0} & \ldots & X_{0,m-1} \\ \vdots & \ldots & \vdots & \ldots & \vdots \\ X_{n-1,-m+1} & \ldots & X_{n-1,0} & \ldots & X_{n-1,m-1} \end{bmatrix} \tag{15}$$

The frequency domain representation is used for a coarse signal search. The procedure looks for candidates in the frequency domain, i.e., columns in matrix (15), where there is a *local Signal-to-Noise Ratio (SNR) maximum*, see [12]. Using the corresponding frequencies as candidate carriers, refined signal paths are searched. A path is defined by a *signal tracking function* $f_\theta : \{0 \ldots n-1\} \mapsto \{-m+1 \ldots 0 \ldots m-1\}$, where θ is a parameter of f. Let Φ denote the set of all instances of such signal tracking functions (assume it is finite size, i.e., there is a finite number of functions and the domains of their parameters are finite).

Example 1 *Tracking of a signal not subject to the Doppler effect, i.e., its frequency is not drifting, is represented by a constant function $f(i) = c$, where i is the half-symbol index and c is the carrier frequency.*

Example 2 *Tracking of a signal subject to a Doppler effect such that the carrier frequency is drifting linearly, is represented by function $f_\delta(i) = c + \delta i$. The parameter δ represents the quantity of frequency drift per half symbol.*

Example 3 *Tracking of a signal subject to a Doppler effect such that the carrier frequency is drifting nonlinearly, is represented by an arbitrary function. The number of possibilities is $(2m-1)^n$, i.e., exponential. An approach for handling this case is further discussed in Section 5.*

For each candidate signal, defined by a signal tracking function f_θ, this step finds a coarse time offset, from the start of a two minute interval. Each candidate signal is examined. A complete frame can start anywhere from the beginning to a time delay corresponding to nine seconds (26 half symbols) into the interval. Let $W_{i,j} = |X_{i,j}|$ denote the magnitude spectrum at indices i and j. For signal

tracking function f_θ, the timing offset τ is the value in the range $0, \ldots, 26$ that maximizes the sum:

$$\sum_{i=1+\tau}^{162} (2s_i - 1) \left[\frac{(W_{i,f_\theta(i)-4} + W_{i,f_\theta(i)+1}) - (W_{i,f_\theta(i)-4} + W_{i,f_\theta(i)+1})}{\sum_{k=-4,-1,1,4} |W_{i,f_\theta(i)+k)}|} \right]$$

The summation measures the correlation of the spectrum power around frequency $f_\theta(i)$ with the synchronization bit-string s. The multiplicand $2s_i - 1$ maps the synchronization bit s_i, which is 0 or 1, to value -1 or 1. The term $W_{i,f_\theta(i)-4} + W_{i,f_\theta(i)+1}$ is the sum of the power at the frequencies of synchronization bit value 1, while the term $W_{i,f_\theta(i)-4} + W_{i,f_\theta(i)+1}$ is the sum of the power at the frequencies of synchronization bit value 0. The denominator represents the sum of all power around frequency $f_\theta(i)$. The power at synchronization bits is relativized to all the power at the candidate frequency.

For each signal tracking function f_θ, over a symbol interval of length T, the power is summed to obtain the energy ($f = -2.2, -0.7, 0.7, 2.2$):

$$r_{i,f} + \sqrt{-1} q_{i,f} = \sum_{t=iT+\tau}^{(i+1)T+\tau} x_t \cdot e^{-\sqrt{-1} 2\pi [f_\theta(t) \cdot 0.73 + f] t} \tag{16}$$

Which is mapped to a magnitude $P_{i,f} = |r_{i,f} + \sqrt{-1} q_{i,f}|$. The four magnitudes $P_{i,f}$ are used to calculate soft symbols. A soft symbol represents a value and its quality. Receive quality metrics are associated with the symbols. This information is used in the decoding process. The most likely symbols are selected first. A de-interleaving procedure reorders the 162 data soft symbols. The resulting 162 soft symbols are passed to a FEC decoder. This part is exactly as originally defined in [12].

5 Evaluation

The exponential search space of the nonlinear case (Example 3) poses a practical problem of time complexity. We resolve this issue making assumptions about the mobility profiles of the vehicles. The Doppler effect is an issue relative to two vehicles, a transmitter and a receiver. In the underwater environment, assumptions can be made about their positions, trajectories and speeds. It is reasonable to assume self position and speed awareness [17]. It is also plausible to suppose that a peer is travelling along a sea route or a navigation channel. Assumptions can also be made regarding its speed [3]. Hence, a straight line model, as discussed in Section 3, can be used to make tractable the problem of searching nonlinearly drifting signals. The search space, i.e., the size of the signal tracking function set Φ, is limited to a number of plausible trajectories. The trajectory model of Equation (6) is applied with assumptions with respect to the domains for the slopes of the lines (m_a, m_b), constants (c_a, c_b), positions of

the vehicles $(\bar{\boldsymbol{a}}, \bar{\boldsymbol{b}})$ and speeds (v_a, v_b). Corollary 1 is applied. Assuming ranges of values for parameters in Equation (6), the Doppler shift-handling aspect of the decoding search strategy is summarized in Figure 2. Three embedded loops generate plausible mobility tuples (m_a, v_a, x, y) for vehicle a including a slope m_a in the interval $[m_{min}, m_{max}]$, a velocity v_a in $[v_{min}, v_{max}]$ and a position (x, y) in $[(x, y)_{min}, (x, y)_{max}]$. The corresponding signal tracking function f_θ is produced and used in the energy search (Equation (16)) and demodulation. We simulated the following three cases for a transmitter and a receiver moving following the motion model presented in Section 3: (i) transmissions without any Doppler shifts (base case); (ii) transmissions with linear Doppler shifts; (iii) transmissions with nonlinear Doppler shifts. The data set used to evaluate the nonlinear case is pictured in Figure 3. Each curve represents the frequency drift captured by one of the individual nonlinear test. It plots the carrier frequency (within 1496 Hz and 1502 Hz) as a function of time, from zero to 120 seconds. Speed varies from five to 10 km/h. Light color is 5 km/h and as you go darker it increases to 10 km/h. The 10 curves close together are due to variation in x ordinate. Trajectories in the Euclidean plane are pictured in Figure 4. Each trace of hollow circles represents a transmitter trajectory, together with the start position (red star). Start coordinate x is varied from -800 m to one km in steps 100 m. Start coordinate y is always zero. The receiver (blue star) is fixed at the origin. The results of the evaluation are shown in Figure 5. The plots show our estimates when there is no Doppler shift (base), linear Doppler shift and nonlinear Doppler shifts during reception of a frame. 300 packets were sent to obtain each data point. The base an linear cases data points were obtained using the original receiver in Ref [12]. The nonlinear case data points were obtained using the receiver described in this paper. According to our simulations, our protocol can operate from the -25 dB SNR range (assuming a 2.5 kHz noise bandwidth). Compared with the data obtained in other research [18], SNRs well above zero are required to obtain similar performance. For equivalent Packet Error Rate

Algorithm 1 The new operations of the protocol decoder

```
for m_min < m_a < m_max                          // slope search
  for v_min < v_a < v_max                        // velocity search
    for (x,y)_min < (x,y) < (x,y)_max            // position search
      find the best tuple (m_a, v_a, x, y)
      use the tuple to identify candidate signals w.r.t. energy & frequency search
      store candidate signals as f_θ
      use f_θ w.r.t. time & demodulation // time resolution & signal demodulation
    end for
  end for
end for
```

Fig. 2. Trajectory parameter enumeration of the decoding search strategy.

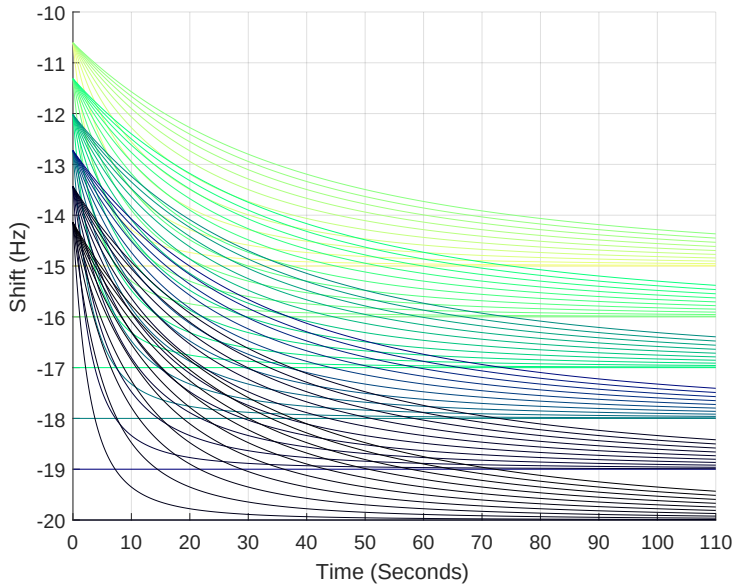

Fig. 3. Curves representing the frequency drift captured by one of the test cases.

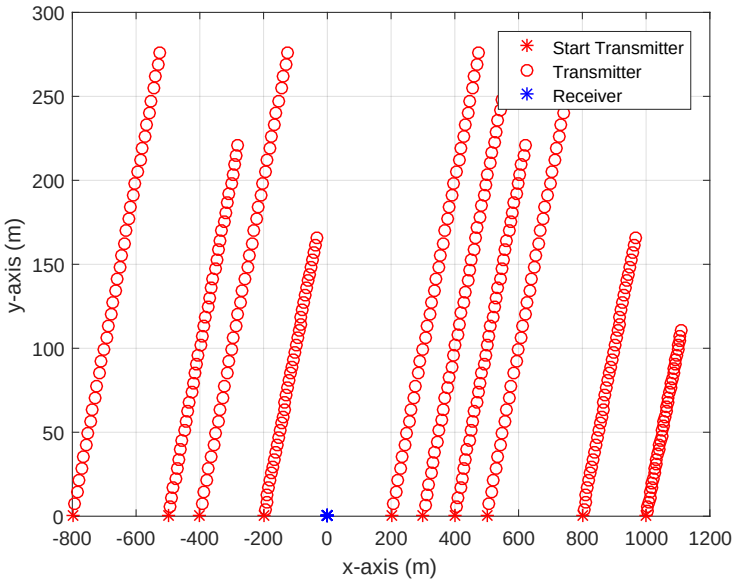

Fig. 4. Evaluated trajectories of transmitter and location of receiver.

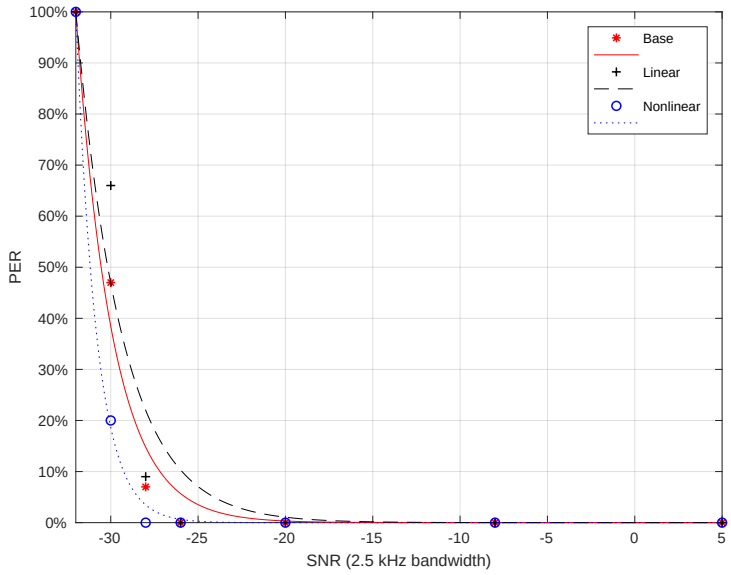

Fig. 5. PER versus SNR for the base case (no Doppler).

(PER) performance and equivalent noise conditions, our protocol can operate with weaker signals. Of course, our data rate is much lower (0.5 bps) and packets are very short (50 bits of data). Using curve fitting, a performance model is produced, see Table 1. The PER as a function of the SNR is modelled with function $f(x) = e^{-\beta(x+32)}$, were x is the SNR. Values for parameter β and 95% confidence bounds are provided.

Table 1. Coefficients of performance model $f(x) = e^{-\beta(x+32)}$.

Case	β (with 95% confidence bounds)
Base	$0.4778\ (0.3527, 0.6029)$
Linear	$0.3787\ (0.2021, 0.5552)$
Noninear	$0.84\ (0.7453, 0.9346)$

6 Conclusion

We have extended a receiver design for low frequency underwater acoustic communications [12] to address Doppler shift patterns identified in [9,10]. The new receiver handles nonlinearly variable Doppler shifts under the assumption of a straight line trajectory model with ranges of plausible parameters. They produce nonlinearly variable Doppler shift patterns. Source code and examples are available online: https://github.com/michelbarbeau/gr-uwspr./

References

1. R. Otnes, J. E. Voldhaug, and S. Haavik. On communication requirements in underwater surveillance networks. In *OCEANS 2008-MTS/IEEE Kobe Techno-Ocean*, pages 1–7. IEEE, 2008.
2. Roald Otnes, Alfred Asterjadhi, Paolo Casari, Michael Goetz, Thor Husøy, Ivor Nissen, Knut Rimstad, Paul Van Walree, and Michele Zorzi. *Underwater acoustic networking techniques*. Springer Science & Business Media, 2012.
3. Robert W. Button, John Kamp, Thomas B. Curtin, and James Dryden. A survey of missions for unmanned undersea vehicles. RAND National Defense Research Institute, 2009.
4. Wikipedia. Underwater locator beacon. https://en.wikipedia.org/wiki/Underwater_locator_beacon, 2018.
5. J. Decarpigny, B. Hamonic, and O. Wilson. The design of low frequency underwater acoustic projectors: present status and future trends. *IEEE Journal of Oceanic Engineering*, 16(1):107–122, 1991.
6. E. Hixson. A low-frequency underwater sound source for seismic exploration. *The Journal of the Acoustical Society of America*, 126(4):2234–2234, 2009.
7. M. Stojanovic. On the relationship between capacity and distance in an underwater acoustic communication channel. *SIGMOBILE Mob. Comput. Commun. Rev.*, 11(4):34–43, October 2007.
8. L. Freitag, J. Partan, P. Koski, and S. Singh. Long range acoustic communications and navigation in the arctic. In *OCEANS 2015 - MTS/IEEE Washington*, pages 1–5, October 2015.
9. Abdel-Mehsen Ahmad, Michel Barbeau, Joaquin Garcia-Alfaro, Jamil Kassem, Evangelos Kranakis, and Steven Porretta. Doppler effect in the underwater acoustic ultra low frequency band. In *Proceedings of the 9th EAI International Conference on Ad Hoc Networks*, Niagara Falls, Canada, 2017. Springer.
10. Abdel-Mehsen Ahmad, Michel Barbeau, Joaquin Garcia-Alfaro, Jamil Kassem, Evangelos Kranakis, and Steven Porretta. Doppler effect in the acoustic ultra low frequency band for wireless underwater networks. *Mobile Networks and Applications*, 2018. https://doi.org/10.1007/s11036-018-1036-9.
11. R. Fano. A heuristic discussion of probabilistic decoding. *IEEE Transactions on Information Theory*, 9(2):64–74, April 1963.
12. Michel Barbeau. Weak signal underwater communications in the ultra low frequency band. In *Proceedings of the 7th GNU Radio Conference*, pages 1–8, San Diego, CA, U.S.A., 2017. https://pubs.gnuradio.org/index.php/grcon/article/view/20/14.
13. B. Wu. A correction of the half-power bandwidth method for estimating damping. *Archive of Applied Mechanics*, 85:315–320, 2015.
14. J. Taylor and B. Walker. WSPRing around the world. *QST*, 94(10):30–32, November 2010.
15. S. Franke and J. Taylor. WSPR, 2017. [Online; accessed 9-May-2017].
16. P Karn. Convolutional decoders for amateur packet radio. In *ARRL Digital Communications Conference*, pages 45–50, 1995.
17. B.S. McCartney. Underwater acoustic positioning systems: State of the art and applications in deep water. *International Hydrographic Review*, LVIII(1):91–113, January 1981.
18. S. Blouin and M. Barbeau. An experimental baseline for underwater acoustic broadcasts. In *2017 IEEE 86th Vehicular Technology Conference (VTC-Fall)*, pages 1–5, September 2017.